Improving the Performance of Perovskite Solar Cells using a Polyphosphazene Interfacing Layer

Bekele Hailegnaw, Vanessa Poscher, Christoph Ulbricht, Hathaichanok Seelajaroen, Ian Teasdale, Yolanda Salinas, Niyazi Serdar Sariciftci, and Markus Clark Scharber*

Herein, the impact of thin layer of polyphosphazene derivatives, as a buffer layer between the electron-transporting layer and the back metal-contact in mixed-cation mixed-halide perovskite solar cells (PSCs), is explored. PSCs with a poly[bis(allylamino)phosphazene] (PPz) interlayer exhibit enhanced rectification in the photo-induced current density–voltage (J–V) curves, which show improved photovoltaic performance and photostability with reduced hysteresis. The thickness of the interlayer is optimized and the optimized PSCs with PPz buffer layer shows an average open-circuit voltage (V_{OC}) of ≈1.05 V, a short-circuit current density (J_{SC}) of around 23.5 mA cm^{-2}, a fill factor of ≈72%, and a power conversion efficiency of about 17.3% for the forward and reverse scans under simulated AM1.5G illumination. Moreover, the application of PPz as an electron-transporting interlayer in organic solar cells reveals that PPz interfacial layer improves the electron extraction at the cathode. The merit of applying PPz interlayer extends to the possibility of using different metals (such as aluminum, gold, copper, and silver) as the top contact in the prepared PCSs. In general, these experiments reveal a very promising approach to tackle the issue of interfacing, and to improve the performance and stability of PSCs.

1. Introduction

Hybrid organic–inorganic perovskite solar cells are a highly growing field of scientific research. Hybrid organic–inorganic perovskite materials possess several appealing properties in particular solution processability, high absorption coefficients, low exciton binding energy, long carrier diffusion lengths (arising from high mobilities and long charge lifetimes), high structural defect tolerance, insensitivity towards intrinsic defects, and benign grain boundary effects. The bandgap can be tuned within

a broad range by changing the composition of the semiconductor materials.[1–4] Due to their outstanding properties, hybrid organic–inorganic perovskite materials form a promising new class of semiconductors for optoelectronic applications, such as photovoltaics and photodetectors, light emission, X-ray imaging, lasers, gamma-ray detection, subwavelength photonic devices in long-wavelength region, etc.[5–10]

The first perovskite solar cell (PSC) was reported by Miyasaka et al. in 2009 with a power conversion efficiency (PCE) of about 3.8%.[11] Since then the progress in optimizing film growth, interface characteristics, and the composition of absorber materials has lead to high-performance photovoltaic devices. For PSCs PCEs up to 23.3% have been reported.[12–15] Almost all reported high-efficiency records utilizing a mesoporous TiO$_x$ layer deposited between the transparent front contact and the absorber layer.[16,17] Depending on the employed layer sequence, planar PSCs can have either inverted p-i-n or regular n-i-p configuration. Inverted PSCs have a hole transporting layer (HTL) deposited on the transparent contact, followed by the perovskite absorber, an electron transport layer (ETL), and a metal electrode contact. In the regular configuration (n-i-p), the layers are deposited in reverse sequence, starting with an ETL layer coated on top of the transparent electrode.[18–21]

The current PCE record reported for PSCs build in the inverted p-i-n configuration is about 20%.[22–24] By suppressing charge carrier recombination and improving the charge extraction efficiency at the interfaces, the PCE of p-i-n PSCs could be further improved. An interface modification of ETL and HTL is essential to optimize the energy-level alignment for efficient electron and hole extraction, ensuring good ohmic contact, and improving the overall performance of the device.[25–27]

Interfacial modifications can also help in improving the device stability and reduce the hysteresis, often found when recording current density–voltage (J–V) curves.[28–30] [6,6]-Phenyl-C$_{61}$ butyric acid methyl ester (PCBM) is one of the most commonly used ETL in PSCs with p-i-n configuration. It fulfills a vital role by passivating charge trap states and by protecting the metal electrode from direct contact with the corrosive perovskite material. When additional layers need to be deposited, the PCBM also

B. Hailegnaw, Dr. C. Ulbricht, H. Seelajaroen, Prof. N. S. Sariciftci, Prof. M. C. Scharber
Linz Institute for Organic Solar Cells (LIOS)
Institute of Physical Chemistry
Johannes Kepler University Linz
Altenberger Straße 69, Linz 4040, Austria
E-mail: markus_clark.scharber@jku.at

V. Poscher, Prof. I. Teasdale, Dr. Y. Salinas
Institute of Polymer Chemistry (ICP) and Linz Institute of Technology (LIT)
Johannes Kepler University Linz
Altenberger Straße 69, Linz 4040, Austria

ADVANCED
SCIENCE NEWS
www.advancedsciencenews.com

physica **pss** **a**
status solidi
www.pss-a.com

protects the perovskite absorber from direct exposure to the processing solvents.[24,31,32]

However, forming an ohmic contact between PCBM and metals deposited by thermal evaporation can be quite challenging.[33–35] To overcome this issue and to improve the charge carrier extraction across the interface between PCBM and the metal contact, many efforts have been undertaken. Introducing an additional buffer layer between the ETL and the back metal-contact has proven to improve the performance and stability of devices. Different buffer layer materials have been reported including inorganic compounds, such as TiO_x, ZnO, LiF, MgF_2, Cr/Cr_2O_3, etc., and organic materials, such as poly(2-ethyl-2-oxazoline) (PEOz) and 2,9-dimethyl-4,7-diphenyl-1,10-phenanthroline (BCP) as well as fullerene C_{60} derivatives.[35–38]

Applying a TiO_x interlayer between the PCBM ETL and the Al contact electrode has proven to improve the photovoltaic performance and stability of PSCs by facilitating electron injection, and blocking ion migration from the photoactive material to the Al electrode.[39,40] Chen et al. showed the enhancement of charge carrier extraction kinetics, and improvement in open circuit voltage, fill factor (FF), and other photovoltaic parameters by applying PEOz between PCBM and Ag contact electrode.[35]

Polyphosphazenes are a family of inorganic–organic molecular hybrid polymers with a covalently linked phosphorus–nitrogen backbone, functionalized with two (commonly organic) substituents on the phosphorus atoms to give poly(organo)phosphazenes.[41] Poly(organo)phosphazenes represent a versatile family of polymers and possess disperse array of properties and thus applications ranging from biodegradable materials for tissue engineering[42] and drug delivery through to polymer electrolyte membranes,[43,44] flame-retardant composites, or as stimuli-responsive materials.[45,46]

In this study, a thin layer of a polyphosphazene derivative is used in the fabrication of PSCs and organic solar cells. It is used as a thin interfacing layer between PCBM ETL and different metal contacts (Cu or Al). We reveal that mixed-cation mixed-halide perovskite $(Cs_{0.5}(FA_{83}MA_{17})_{0.95}PbI_{3-x}Br_x)$ solar cells with poly[bis(allylamino)phosphazene] (PPz) as an ETL interlayer show improved rectification in the J–V) curve and reduced hysteresis, resulting in higher FF, PCEs, and device stabilities. Atomic force microscopy (AFM) topographic imaging shows that the deposition of a PPz thin film on top of PCBM leads to smoother surfaces. Electrochemical impedance spectroscopy (EIS), intensity-modulated photo-voltage spectroscopy (IMVS), photoluminescence (PL), and PL-decay spectroscopy investigations show the improvement of charge carrier dynamics in the bulk and across interfaces, and the reduction of recombination when PPz is used as buffer layer. Furthermore, to verify the charge-transporting preference, PPz was tested as buffer layer as a hole- and electron-transporting interlayer in bulk-heterojunction solar cells (BHJSCs) based on a blend solution of poly(3-hexylthiophene-2,5-diyl) (P3HT) and PCBM. The results indicate that the used PPz compound plays a vital role in the electron extraction process.

2. Results and Discussion

Figure 1a shows the molecular structure of PPz ($n \sim 5$), called "PPz5" here after. The polymer was prepared by phosphine-mediated living polymerization and the details of synthesis for different derivatives are shown in the supporting information (SI).[47] PPz5 was used as an interlayer between the ETL, PCBM, and the back metal-contact as shown in **Figure 2**a, which shows the schematic architecture of an inverted (p-i-n) PSCs. PPz ($n \sim 50$) and hexa(allylamino)cyclotriphosphazene were also applied similarly and compared with PPz5 in SI and in Figure SI-4, Supporting Information.

To examine the energetics of PPz5, the electrochemical properties of the compound were probed by means of cyclic voltammetry. Acetonitrile containing 0.1 M tetrabutylammonium hexafluorophosphate was applied as a supporting electrolyte and experiments were performed under N_2-saturated condition. The three-electrode setup was equipped with an indium tin oxide (ITO)-coated glass as a working electrode, a Pt plate counter electrode, and a Ag/AgCl quasi-reference electrode.

Cyclic voltammograms (CVs) of PPz5 were recorded at potentials between 0 and -1.0 V in the cathodic range, and from 0 to 2.0 V in the anodic range with a scan rate of 10 mV s^{-1}, as shown in Figure 1b,c. The onset potentials were calibrated with a ferrocene/ferrocenium couple using 0.69 V versus normal hydrogen electrode (NHE),[48] and the Equation (1) and (2) were used to estimate the highest occupied molecular orbital (HOMO) and the lowest unoccupied molecular orbital (LUMO) energy levels (E_{HOMO} and E_{LUMO}).[49,50] The results suggest E_{HOMO} at around -6.5 ± 0.1 eV, and E_{LUMO} in the range of -4.2 ± 0.1 eV, which are in a reasonable agreement with the optical bandgap derived from the absorption spectrum (Figure 1d). The LUMO position suggests that PPz5 is a suitable interfacial material to be applied between the PCBM and the top contact. In Figure 2b, the band diagram of the investigated device structure is shown.

$$E_{HOMO} = -(E_{[ox,onset-vs-NHE]} + 4.75)\,eV \tag{1}$$

$$E_{LUMO} = -(E_{[red,onset-vs-NHE]} + 4.75)\,eV \tag{2}$$

3. Current Density-vs-Voltage Response

Figure 2a displays the schematic structure of the investigated p-i-n PSCs. Figure 2c shows the J–V characteristics of mixed-halide mixed-cation PSCs with and without PPz5 buffer layer under 100 mW cm^{-2} light-intensity illumination (AM1.5 global spectrum) and Figure 2d shows the J–V characteristics under dark conditions in a semi-log plot. The PPz5 interlayer was processed from a 0.5 mg mL^{-1} solution in IPA. The photovoltaic parameters calculated from the J–V curves are shown in **Table 1**. Devices with PPz5 interlayer show improved FF and PCE compared with devices without PPz5 interlayer. PSCs with PPz5 interlayer exhibit improved rectification, and reduced series resistance and less leakage current (Figure 2d).

To optimize and investigate the impact of PPz5 layer thickness on the performance of PSCs, different concentrations of PPz5 (i.e., 0.25, 0.5, 1, 2, and 5 mg mL^{-1} in IPA) were used in the device fabrication. The thickness of the resulting thin films

ADVANCED
SCIENCE NEWS
www.advancedsciencenews.com

physica
pss
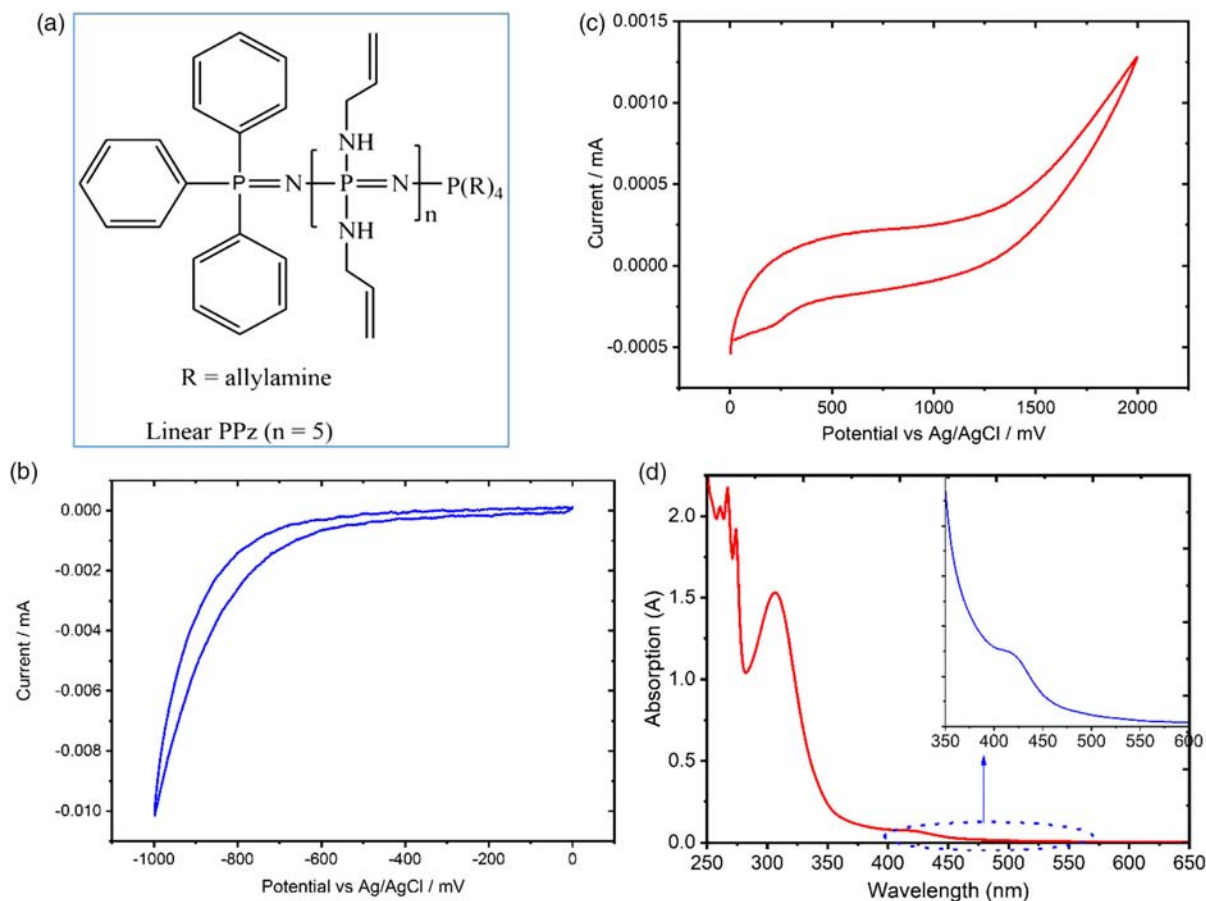status solidi a

www.pss-a.com

Figure 1. a) Chemical structure of linear poly[bis(allylamino)phosphazene] (PPz5). b) Reductive and c) oxidative cyclic voltammogram of PPz5 in acetonitrile (4 mg mL^{-1}) containing tetrabutylammonium hexafluorophosphate (0.1 M) as a supporting electrolyte using ITO as working electrode, Ag/AgCl reference electrode and Pt counter electrode. d) UV-Vis absorption spectrum of PPz5 solution in IPA.

was measured using a profilometer (Bruker Dektak XT) which show thicknesses in the range of 5 to 30 nm. Figure 2e shows the J–V curves of perovskite devices with PPz5 interlayer of different thickness. The open-circuit voltage (V_{OC}) of the devices decreases as the concentration of employed PPz5 increases. Devices with buffer layers fabricated from 1 and 2 mg mL^{-1} PPz5 solution exhibit the highest short-circuit current density (J_{SC}), an FF, and the best PCE. The external quantum efficiency spectra in Figure 2f also confirm that devices with 1 and 2 mg mL^{-1} PPz5 show the highest EQE and integrated J_{SC}. However, already after one night stored within a nitrogen glove box, devices prepared with 2 mg mL^{-1} PPz5 solution showed substantial loss in J_{SC}, FF, and overall efficiency. In contrast, devices based on 1 mg mL^{-1} PPz5 solution, which has a PPz5 layer thickness of about 10 to 15 nm, remained stable (Figure SI-5, Supporting Information). Consequently, we used 1 mg mL^{-1} PPz5 solution as the optimum concentration for further characterization. Devices with 5 mg mL^{-1} PPz show the least photovoltaic properties and the EQE spectrum was not measured.

To study the surface modification induced by PPz5 interlayers, AFM topographic images were recorded for different samples. The surface topographies of a mixed-cation mixed-halide perovskite (PVS) film, a PVS coated with PCBM, and a mixed-cation mixed-halide perovskite film/PCBM stack covered with PPz5 are compared **(Figure 3)**. All samples were deposited on ITO-coated substrates coated with NiO$_x$ thin-films to mimic the interfaces in the PSCs. Films covered with PCBM (Figure 3b) show improved surface smoothness when compared with pristine perovskite films (Figure 3a). The root-mean-square (RMS) roughness value is reduced from about 57 nm for a pristine perovskite film to ≈7 nm when coated with PCBM. This suggests good surface coverage of the perovskite film with PCBM. A subsequent deposition of PPz5 on top of PCBM increases the surface smoothness further (Figure 3c), and the RMS roughness is reduced to around 6.6 nm. This indicates that PPz5 layer forms a homogenous overcoat over the ETL which could heal defects in PCBM film, and reduces the probability of direct contact between the photoactive layer and the back electrode.

Room temperature PL characterization of the perovskite films and films with and without PPz5 interlayer was conducted. **Figure 4**a shows the PL spectra of mixed-cation mixed-halide perovskite (PVS) films, PVS coated with PCBM (PVS/PCBM), and PVS/PCBM films covered with PPz5 (i.e., PVS/PCBM/PPz5). The PL of films with PPz5 on top of PCBM (PVS/PCBM/PPz5) shows more quenching when compared with films
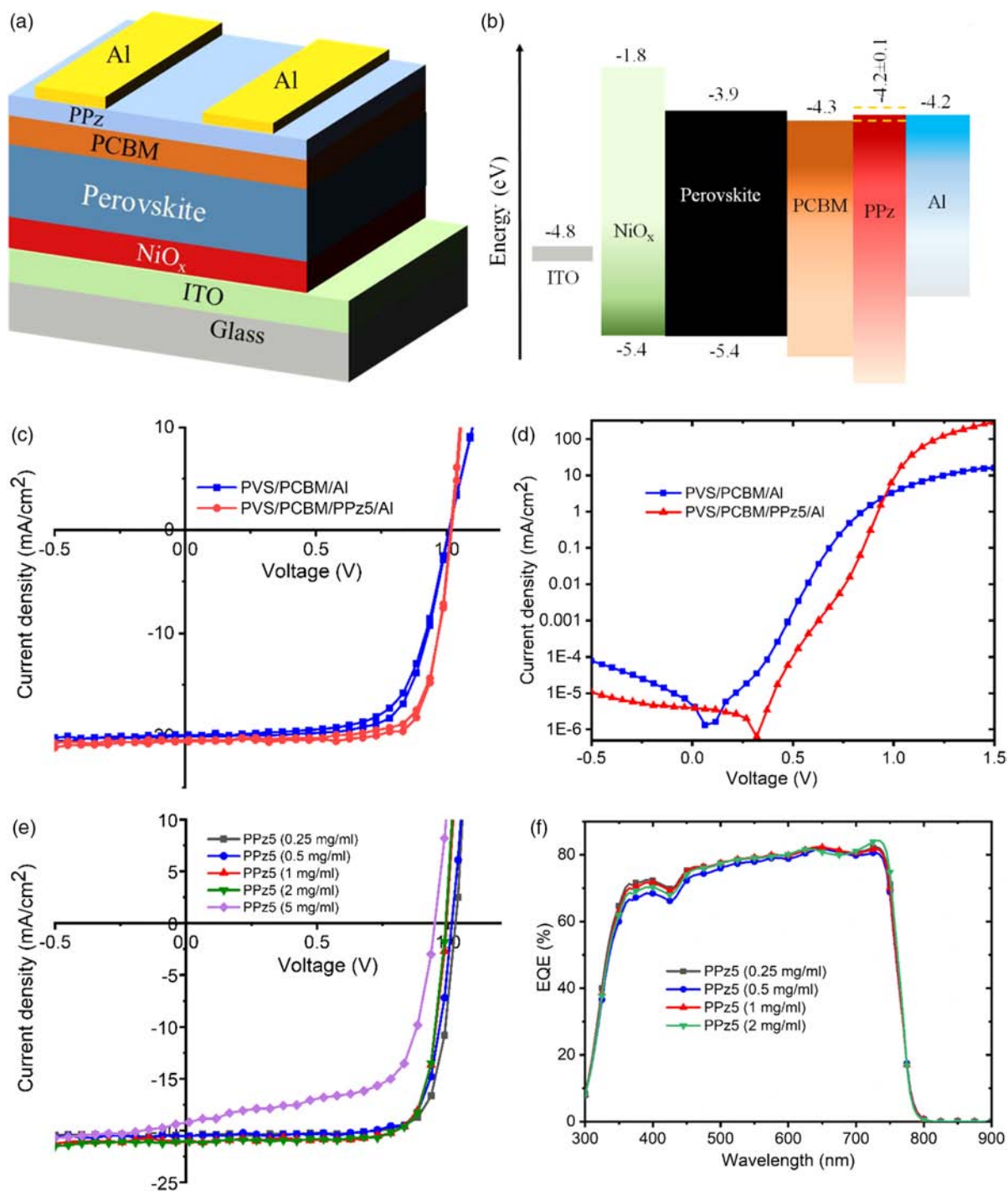
Figure 2. a) Schematic structure of PSCs with polyphosphazene interlayer and b) corresponding energy diagram of the respective layers in the cells.[51,52] Characteristic current density–voltage (*J*–*V*) response of PSCs with (red) and without (blue) PPz5 interlayer c) under 1 sun light (AM1.5 solar spectrum) illumination and (d) in the dark(semi-log plot). e) Current density–voltage (*J*–*V*) characteristic of PSCs prepared with 0.25, 0.5, 1, 2, and 5 mg mL^{-1} PPz5 solutions under 1 sun light illumination, and f) external quantum efficiency and integrated *J*$_{SC}$ calculated from the EQE data.

without PPz5 layer. This could indicate the improvement of charge-carrier-transfer dynamics from the photoactive film to the ETL. Similarly in the PL-decay spectra (Figure 4b), films with PPz5 interlayer show faster PL decay as compared with films

without PPz5 interlayer. This might indicate the reduction of charge trapping states at the ETL interface.

To gain insight on the compatibility of PPz5 buffer layer with different back metal-contact, PSCs with Al, Au, and Cu back

Table 1. Summarized photovoltaic parameters (i.e., V_{OC}, J_{SC}, FF, and PCE) of PSCs given in Figure 2b,c for forward (Fwd) and reverse scans (Rvs) under 100 mW cm^{-2} light-intensity illumination.

Type of PSCs	Scan	V_{OC} [V]	J_{SC} [mA cm^{-2}]	FF [%]	PCE [%]
PCBM/Al	Fwd	1.01	19.8	67.6	13.6
	Rvs	1.01	20.2	70.5	14.4
PCBM/PPz5/Al	Fwd	1.02	20.4	75.8	15.7
	Rvs	1.02	20.5	78.7	16.4

metal-contact were fabricated and characterized. The J–V characteristics of selected solar cells show highly similar photovoltaic behavior with only slight deviations (Figure SI-6, Supporting Information). This verifies that PPz5 forms a suitable cathodic interface with these metals electrodes.

Figure 5a,b shows the photovoltaic properties of a PSC with PPz5 buffer layer obtained after subsequent optimization of the devices processing conditions. The photovoltaic parameters of the best-performing solar cell are shown in Figure 5a. The device exhibits a considerably low hysteresis and a PCE of about 16% under 1 sun light (AM1.5 solar spectrum) illumination. The EQE spectrum in Figure 5b shows an EQE of around 88% with integrated short-circuit current density (J_{SC}) of about

21.2 mA cm^{-2}. The statistical distribution of PCE for 129 PSCs with PPz interlayer and 97 PSCs without PPz interlayer shows that the average PCE of sample devices is about 15% higher than the control devices (Figure SI-7, Supporting Information).

To examine the steady-state output of a PSC with PPz5 buffer layer, a maximum power point (MPP) tracking measurement was conducted under 100 mW cm^{-2} simulated AM1.5 solar spectrum illumination. Figure SI-8a, Supporting Information shows the normalized steady state PCE and maximum current-density output (J_{max}) of the same PSCs under 1 sun light illumination for 8 h in a N$_2$ glove box. The normalized MPP voltage (V_{max}), photocurrent density (J_{max}), and the delivered electrical power output (P_{max}) of the device are shown in Figure SI-8b, Supporting Information. All recorded solar cell parameters are fairly stable over the entire recording period.

4. Impedance Spectroscopy

To investigate the impact of the PPz5 buffer layer on the electron dynamics across the bulk and interfaces of PSCs, EIS and intensity-modulated photovoltage spectroscopy (IMVS) were applied. The EIS characteristics of optimized PSC with 1 mg mL^{-1} PPz interlayer and PSC without PPz interlayer (control device) were
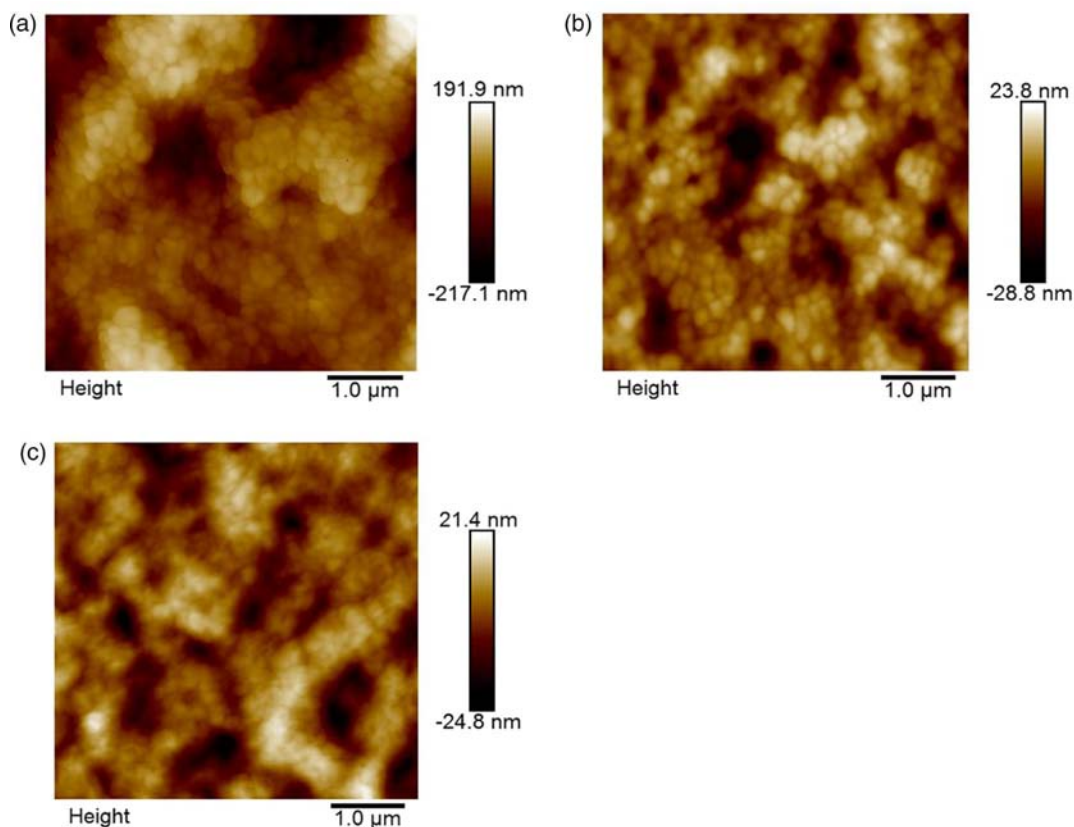

Figure 3. Atomic force microscope images of a) mixed-cation mixed-halide perovskite films, b) mixed-cation mixed-halide perovskite covered with PCBM, and c) mixed-cation mixed-halide perovskite/PCBM coated with PPz5. The films are deposited on ITO coated glass substrate covered with NiO$_x$ nanoparticles.
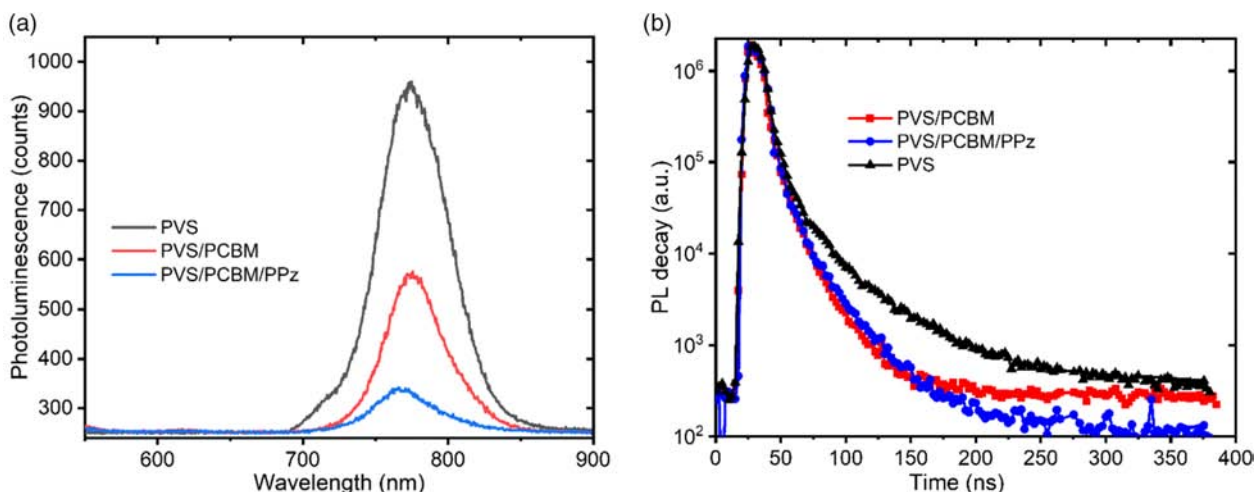
Figure 4. a) Photoluminescence (PL) and b) PL-decay spectra of mixed-cation mixed-halide perovskite (PVS) film, PVS covered with PCBM (PVS/PCBM), and PVS/PCBM coated with PPz5 (PVS/PCBM/PPz5).
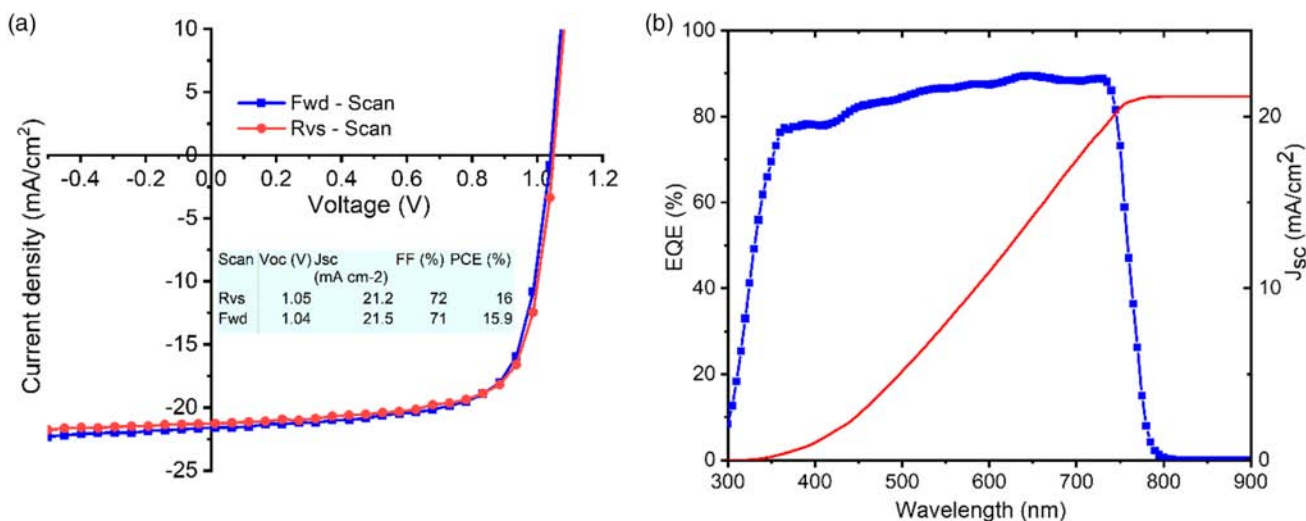

Figure 5. a) J–V curves of optimized PSC with, glass/ITO/NiO$_x$/Cs$_{0.05}$(FA$_{0.83}$MA$_{0.17}$)$_{0.95}$PbI$_{3-x}$Br$_x$/PCBM/PPz5/Al structure under AM1.5 solar spectrum (100 mW cm^{-2} light intensity) illumination. (b) EQE spectrum and the integrated J$_{SC}$ of the optimized PSC.

measured at short-circuit condition with 10 mV AC-voltage in the frequency sweep between 1 MHz and 0.02 Hz under LED light ($\lambda = 590$ nm) illumination. The IMVS response of the same PSCs used in EIS was measured at open-circuit voltage in the frequency range between 1 MHz and 0.02 Hz under 8 mW cm^{-2} LED irradiation ($\lambda = 590$ nm) with light-intensity perturbation (10% modulation amplitude). **Figure 6**a shows the Nyquist plots of the EIS response. The corresponding Bode plots are shown in Figure 6b. Solar cells with buffer layer and PPz5 without buffer layer display two characteristic peaks in their EIS responses. The high-frequency (1 MHz–10 kHz) response is related to charge carrier transport resistance (R2), and the low-frequency (10 Hz–20 mHz) features are associated to impedance of ionic diffusion and trap states (charge recombination) within the

perovskite film and at the interface of the charge transport layers.[53–56]

Based on this approach, an equivalent circuit which describes these EIS responses is suggested in Figure 6c. The fitting parameters for each circuit element are calculated as shown in **Table 2**. Both plots, Nyquist and Bode, and Table 2, show that PSCs with PPz5 interlayer exhibit reduced charge transport resistance (R2 = 44.1 Ω) when compared with the control devices (187.5 Ω). The low-frequency resistance (R3), which is associated with impedance of trap state charge carrier recombination, and ion diffusion at the interface and within bulk, appears reduced for devices with a PPz5 interlayer. Furthermore, in both frequency regions, the capacitive element increases for the sample devices.
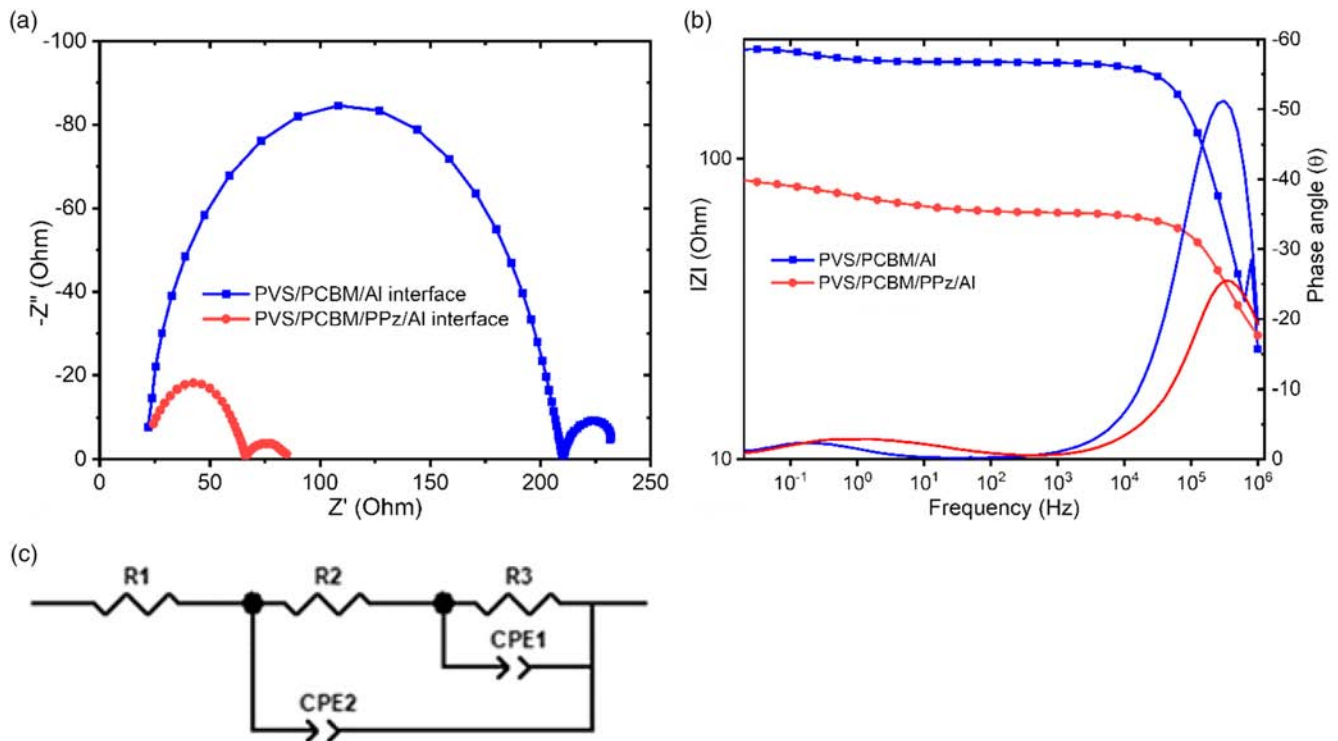
Figure 6. a) Nyquist plots and b) Bode plots of the electrochemical impedance spectroscopy (EIS) response of a PSC with PPz5 buffer layer (PCBM/PPz5/Al, red) and control device (PCBM/Al, blue), scanned in the frequency range of 1 MHz to 20 mHz with 0 V DC voltage and 10 mV AC-voltage under 8 mW cm^{-2} LED light intensity. c) Equivalent circuit model for the solar cells.

Table 2. Equivalent circuit fitting parameters; series resistance (R_1), geometric resistance (R_2), constant-phase element (CPE2) corresponding to the bulk, resistance related to interface (R_3), and interface related constant-phase element (CPE1), extracted from the fitting of EIS response of PSCs with and without PPz5 interlayer.

| | R_1 [Ω] | R_2 [Ω] | CPE1 | | R_3 [Ω] | CPE2 | |
			T [F]	P		T [F]	P
PVS/PCBM/Al	21.2	187.5	0.02897	0.9	23.6	2.48e-8	0.93
PVS/PCBM/PPz5/Al	21.2	44.1	0.235	0.47	21.4	1.05e-7	0.88

The IMVS response of PSCs with and without PPz5 inter-layer are shown as Nyquist plots in Figure SI-9a, Supporting Information, and the complex-transfer function versus frequency response is shown in Figure SI-9b, Supporting Information. Analogous to the EIS characteristics, the high-frequency IMVS response, which is associated with recombination resistance,[54] is higher for PSCs with PPz5 buffer layer. This indicates a reduction of recombination pathways and an improvement of charge carrier extraction processes. The charge carrier life time (τ), as a function of V_{OC}, was calculated from the complex-transfer function versus frequency responses of the devices at different LED light intensities (Figure SI-9c, Supporting Information).

The critical frequency, corresponding to the maximum of complex-transfer function versus frequency plot at high frequency, is related to critical time by, $f_c = \frac{1}{2\pi\tau_c}$.[57]

PSCs with PPz5 buffer layer show longer charge carrier life times when compared with solar cells without a buffer layer. The EIS together with IMVS results suggest that a PPz5 buffer layer reduces the charge carrier transport resistance and improves the recombination resistance leading to longer charge carrier lifetimes and improved photovoltaic behaviors.

5. Organic Solar Cells

Moreover, to investigate the charge carrier selectivity of PPz5, we applied PPz5 buffer layers in P3HT:PCBM-based BHJSCs. We fabricated devices with inverted (n-i-p) configuration as schematically shown in **Figure 7**a. The impact of PPz5 and/ or polyethy-lenimine (PEI) is compared. Figure 7b shows the *J–V* curves of
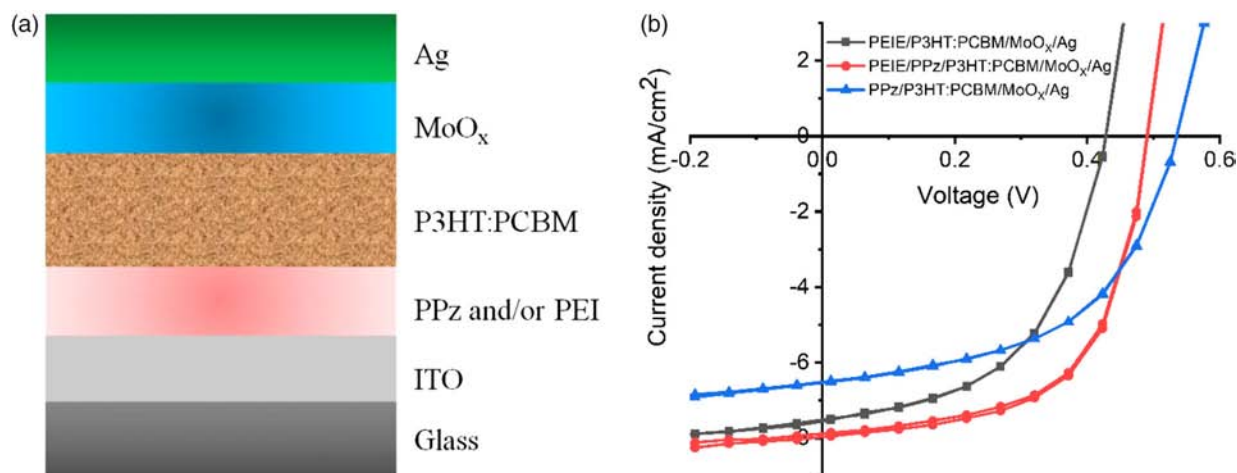
Figure 7. a) Schematic representation of n-i-p bulk-heterojunction solar cells (BHJSCs) with PPz5 and/ or PEI as an electron-transporting layer (ETL) and b) J–V characteristics of P3HT:PCBM-based BHJSCs using PPz5, PEI, or PEI/PPz5 interlayers under 1 sun light illumination.

P3HT:PCBM-based BHJSCs with PPz5, PEI, or PEI/PPz5 as cathodic interlayer. All devices show reasonable J–V characteristics suggesting that PPz5 works as a interfacial layer between the organic semiconductor absorber and the cathode.

6. Conclusion

We fabricated mixed-cation mixed-halide PSCs using polyphosphazene for the first time as a buffer layer between PCBM and back metal-contact. PSCs with PPz5 interlayer show an improved rectification in the J–V characteristics with reduced hysteresis, enhanced photovoltaic properties, and photostability. AFM topographic imaging shows that the addition of PPz5 thin film on the top of PCBM induces morphological modifications. The thickness of the PPz5 interlayer was optimized, and the best PSCs show an average V_{OC} of ≈1.05 V, a J_{SC} of ≈21.2 mA cm^{-2}, an FF of ≈71.5%, and a PCE of ≈16% for the forward and reverse scans under AM1.5 solar spectrum (100 mW cm^{-2}). EIS, PL, and PL-decay spectroscopy investigations reveal improvement of charge carrier dynamics in the bulk and across interfaces, and reduction of recombination. Moreover, IMVS measurements at different LED-light intensities show that devices with PPz5 exhibit about threefold longer charge carrier life time when compared with the devices without buffer layer. The application of PPz5 in organic solar cells proves that it can be used as interfacial layer for the electron extracting process. Furthermore, the merit of interfacing PPz5 has extended to the possibility of using different metal contacts besides Al such as Au, Cu, and Ag. It shows good photovoltaic behavior with substantially the same PV characteristics for different metal contacts. This very first investigation on the application of a polyphosphazene derivative as interlayer material in perovskite and in organic BHJSCs provided highly promising results. Also the vast structural variability inherent within the polyphosphazene family strongly encourages further studies.

7. Experimental Section

Device Fabrication: Glass substrates coated with ITO were sequentially sonicated in acetone, detergent, deionized water, and isopropanol (IPA). A thin layer of nickel oxide (NiO$_x$) nanoparticles was used as a HTL. NiO$_x$ nanoparticles were synthesized following the procedure reported by X. Yin et al.[58] About 20 mg mL^{-1} of NiO$_x$ particles in water were cracked using an ultrasound sonicator (UP50H, 50 W, frequency 30 kHz), followed by filtration through 0.45 μm pore-size polytetrafluoroethylene (PTFE) syringe filter. Then the dispersion was deposited by spin coating (4000 rpm for 15 s and 5000 rpm for 15 s) on the ITO-coated substrate. Subsequently, the film was annealed at 140 °C for 20 min, which resulted in about 40 to 50 nm thick NiO$_x$ thin film. For the deposition of perovskite films and further processing, the substrates were transferred into a glove box.

Mixed-cation mixed-halide perovskite (Cs$_{0.05}$(FA$_{0.83}$MA$_{0.17}$)$_{0.95}$ PbI$_{3-x}$Br$_x$) solutions were prepared by dissolving PbI$_2$ (1.6 mmol), CH(NH$_2$)$_2$I (1.45 mmol), PbBr$_2$ (0.3 mmol), and CH$_3$NH$_3$Br (0.29 mmol) in a mixture of dry N,N-dimethylformamide (DMF) and dimethyl sulfoxide (DMSO) solvent (4:1 (v/v) ratio, 1.5 mL), followed by stirring at 45 °C. Then, 5% (v/v) of CsI from a stock solution (1.5 M in DMSO) was added into the mixture and stirred for about 3 h. The organic salts (CH$_3$NH$_3$Br and CH(NH$_2$)$_2$I) were synthesized following the same synthesis procedure mentioned in our earlier article.[39] The perovskite solution was deposited on top of NiO$_x$ films inside a nitrogen glove box. Spin coating was conducted in two steps at 1500 rpm for 10 s with ramp: 150 rpm s^{-1} and at 6000 rpm for 30 s with ramp: 3000 rpm s^{-1}, with in-situ anti-solvent quenching by dropping about 0.2 mL of chlorobenzene starting at the last 23rd s for about 3 s. Then films were annealed at 100 °C for 1 h. After the samples were cooled down to room temperature; PCBM dissolved in a mixture of chlorobenzene and chloroform (50:50 volume ratio, 2 wt%) was spin-coated on top of the perovskite film. For some devices, PPz5 dissolved in IPA (0.25, 0.5, 1, 2, and 5 mg mL^{-1}) was spin-coated at 5000 rpm for 30 s followed by annealing at 102 °C for about 3 min in the glove box. Devices were finalized by depositing (Al or Cu) through a shadow mask by thermal evaporation at a pressure of ≈10^{-6} mbar.

BHJSCs based on a P3HT:PCBM photoactive blend were fabricated in an n-i-p configuration. A thin layer of PPz5 (1 mg mL^{-1} in IPA) or polyethyleneimine (PEI, 0.2 wt% in n-butanol) were spin-coated on top of cleaned ITO (5000 rpm for 30 s with ramp: 1000 rpm s^{-1}). To check the combined effect of PEI and PPz5, PPz5 was spin-coated on top of PEI (5000 rpm for 30 s with ramp: 2500 rpm s^{-1}). All the films were annealed at 105 °C for 5 min. The photoactive blend solution was prepared

by dissolving P3HT:PCBM (1:1 weight ratio) in chlorobenzene ($20\,mg\,mL^{-1}$) and stirred at $60\,°C$. The solution was spin-coated on top of the buffer layers (1500 rpm for 20 s with ramp: $750\,rpm\,s^{-1}$ and at 2000 rpm for 30 s with ramp: $1000\,rpm\,s^{-1}$) and annealed at $110\,°C$ for 5 min. In a last step, 10 nm of MoO_x and 100 nm of Ag were thermally deposited through a shadow mask by thermal evaporation at a pressure of $\approx 10^{-6}$ mbar.

P-i-n BHJSCs were also fabricated using poly(3,4-ethylenedioxythiophene) polystyrene sulfonate (PEDOT:PSS) or a thin PPz5 film as a HTL. PPz5 was spin-coated and thermally treated as mentioned earlier. PEDOT:PSS was spin-coated (1000 rpm for 3 s with ramp: $500\,rpm\,s^{-1}$ and at 4000 rpm with ramp: $2000\,rpm\,s^{-1}$ for 30 s) and annealed at $120\,°C$ for 15 min. P3HT:PCBM solution was spin-coated and thermally treated the same way as in the case of n-i-p. Solar cells were finished via thermal deposition of a thin anode interlayer (0.8 nm) of LiF, followed by 110 nm of aluminum.

Characterization: The surface morphology of the films was characterized using atomic force microscope (AFM, Bruker Innova). The characteristic photocurrent *J–V* response of the cells was measured with a Keithley-2400-LV source meter. A LOT-QD solar simulator with a 1000 W xenon lamp providing AM1.5 global spectrum was used for irradiation. The intensity of the solar simulator was adjusted using a calibrated silicon reference diode. The external-quantum efficiency (EQE) was measured using an optical setup consisting of a lock-in amplifier (SR830, Stanford Research Systems) and a Jaissle 1002 potentiostat functioning as a preamplifier. Devices were illuminated with light from a xenon lamp passing through a monochromator (Oriel Cornerstone). A filter wheel holding long-pass filters and a mechanical chopper were mounted between the xenon lamp and the monochromator. Chopping frequencies in the range of 10–200 Hz were chosen. A calibrated silicon diode (Hamamatsu S2281) was used as a reference for the light intensity at each wavelength.

EIS characterization was performed under light perturbation in the frequency range of 1 MHz to 0.01 Hz using a SolarLab XM-Potentiostat/Galvanostat (AMETEK). Absorbance, PL-decay, and PL measurements were conducted on various thin film samples. A Perking Elmer 1050 spectrometer was used to measure absorbance. To determine the PL, samples were excited with a COHERENT OBIS 532-150 LS laser (532 nm). The PL emitted from the sample was reflected inside an integrating sphere (HAMAMATSU PHOTONICS, A9924-06). The reflected PL was focused, and transferred by fiber optics to a Shamrock SR-303i monochromator and an Andor™ iDus Si-CCD detector. PL-decay measurements were performed using a Shamrock SR-303i-A monochromator equipped with an intensified charge-coupled device camera (Andor iStar DH320T-18U-73; gate step, 2.5 ns; gate width, 2.5 ns). A Nd:YAG laser (Spit light Compact 100) provided $\approx$10 ns, $\approx$0.1 mJ pulses with a photon energy of 2.33 eV (532 nm).

Supporting Information

Supporting Information is available from the Wiley Online Library or from the author.

Conflict of Interest

The authors declare no conflict of interest.

[1] D. P. McMeekin, G. Sadoughi, W. Rehman, G. E. Eperon, M. Saliba, M. T. Hörantner, A. Haghighirad, N. Sakai, L. Korte, B. Rech, M. B. Johnston, L. M. Herz, H. J. Snaith, *Science* **2016**, *351*, 151.

[2] T.-B. Song, Q. Chen, H. Zhou, C. Jiang, H.-H. Wang, Y. M. Yang, Y. Liu, J. You, Y. Yang, *J. Mater. Chem. A* **2015**, *3*, 9032.

[3] J.-H. Im, I.-H. Jang, N. Pellet, M. Grätzel, N.-G. Park, *Nat. Nanotechnol.* **2014**, *9*, 927.

[4] J. Berry, T. Buonassisi, D. A. Egger, G. Hodes, L. Kronik, Y.-L. Loo, I. Lubomirsky, S. R. Marder, Y. Mastai, J. S. Miller, D. B. Mitzi, Y. Paz, A. M. Rappe, I. Riess, B. Rybtchinski, O. Stafsudd, V. Stevanovic, M. F. Toney, D. Zitoun, A. Kahn, D. Ginley, D. Cahen, *Adv. Mater.* **2015**, *27*, 5102.

[5] D. Yang, R. Yang, K. Wang, C. Wu, X. Zhu, J. Feng, X. Ren, G. Fang, S. Priya, S. (F.) Liu, *Nat. Commun.* **2018**, *9*, 1.

[6] L. Zhao, N. Rolston, K. M. Lee, X. Zhao, M. A. Reyes-Martinez, N. L. Tran, Y.-W. Yeh, N. Yao, G. D. Scholes, Y.-L. Loo, A. Selloni, R. H. Dauskardt, B. P. Rand, *Adv. Funct. Mater.* **2018**, *28*, 1802060.

[7] Z. Xiao, R. A. Kerner, L. Zhao, N. L. Tran, K. M. Lee, T.-W. Koh, G. D. Scholes, B. P. Rand, *Nat. Photon.* **2017**, *11*, 108.

[8] K. Zhang, M. Ma, P. Li, D. H. Wang, J. H. Park, *Adv. Energy Mater.* **2016**, *6*, 8.

[9] S. Chen, K. Roh, J. Lee, W. K. Chong, Y. Lu, N. Mathews, T. C. Sum, A. Nurmikko, *ACS Nano* **2016**, *10*, 3959.

[10] N. Alwadai, M. A. Haque, S. Mitra, T. Flemban, Y. Pak, T. Wu, I. Roqan, *ACS Appl. Mater. Interfaces* **2017**, *9*, 37832.

[11] A. Kojima, K. Teshima, Y. Shirai, T. Miyasaka, *J. Am. Chem. Soc.* **2009**, *131*, 6050-6051.

[12] H.-S. Kim, C.-R. Lee, J.-H. Im, K.-B. Lee, T. Moehl, A. Marchioro, S.-J. Moon, R. Humphry-Baker, J.-H. Yum, J. E. Moser, M. Grätzel, N.-G Park, *Sci. Rep.* **2012**, *2*, 1.

[13] NREL, Efficiency chart, **2018**, https://www.nrel.gov/pv/assets/pdfs/pv-efficiency-chart.20181221.pdf (accessed: January 2019).

[14] W. S. Yang, B.-W. Park, E. H. Jung, N. J. Jeon, Y. C. Kim, D. Uk Lee, S. S. Shin, J. Seo, E. K. Kim, J. H. Noh, S. Il Seok, *Science* **2017**, *356*, 1376.

[15] H. Chen, F.I Ye, W. Tang, J. He, M. Yin, Y. Wang, F. Xie, E. Bi, X. Yang, M. Grätzel, L. Han, *Nature* **2017**, *550*, 92.

[16] Y. Hou, X. Du, S. Scheiner, D. P. McMeekin, Z. Wang, N. Li, M. S. Killian, H. Chen, M. Richter, I. Levchuk, N. Schrenker, E. Spiecker, T. Stubhan, N. A. Luechinger, A. Hirsch, P. Schmuki, H.-P. Steinrück, R. H. Fink, M. Halik, H. J. Snaith, C. J. Brabec, *Science* **2017**, *358*, 1192.

[17] G. Adam, M. Kaltenbrunner, E. D. Głowacki, M. S. White, H. Heilbrunner, S. Tombe, P. Stadler, N. S. Sariciftci, M. C. Scharber, *Sol. Energy Mater. Sol. Cells* **2016**, *157*, 318.

[18] J. H. Heo, H. J. Han, D. Kim, T. K. Ahn, S. H. Im, *Energy Environ. Sci.* **2015**, *8*, 1602.

[19] K. Jäger, L. Korte, B. Rech, S. Albrecht, *Opt. Express* **2017**, *25*, A473.

[20] K. A. Bush, A. F. Palmstrom, Z. J. Yu, M. Boccard, R. Cheacharoen, J. P. Mailoa, D. P. McMeekin, R. L. Z. Hoye, C. D. Bailie, T. Leijtens, I. M. Peters, M. C. Minichetti, N. Rolston, R. Prasanna, S. Sofia, D. Harwood, W. Ma, F. Moghadam, H. J. Snaith, T. Buonassisi, Z. C. Holman, S. F. Bent, M. D. McGehee, *Nat. Energy* **2017**, *2*, 17009.

[21] A. Magomedov, A. Al-Ashouri, E. Kasparavičius, S. Strazdaite, G. Niaura, M. Jošt, T. Malinauskas, S. Albrecht, V. Getautis, *Adv. Energy Mater.* **2018**, *8*, 1801892.

[22] J. H. Heo, S.-C. Lee, S.-K. Jung, O.-P. Kwon, S. H. Im, *J. Mater. Chem. A* **2017**, *5*, 20615.

[23] Y. Wu, F. Xie, H. Chen, X. Yang, H. Su, M. Cai, Z. Zhou, T. Noda, L. Han, *Adv. Mater.* **2017**, *29*, 1701073.

[24] S. Ye, H. Rao, Z. Zhao, L. Zhang, H. Bao, W. Sun, Y. Li, F. Gu, J. Wang, Z. Liu, Z. Bian, C. Huang, *J. Am. Chem. Soc.* **2017**, *139*, 7504.

[25] G. Yang, C. Wang, H. Lei, X. Zheng, P. Qin, L. Xiong, X. Zhao, Y. Yan, G. Fang, *J. Mater. Chem. A* **2017**, *5*, 1658.

[26] M. Ye, C. He, J. Iocozzia, X. Liu, X. Cui, X. Meng, M. Rager, X. Hong, X. Liu, Z. Lin, *J. Phys. D: Appl. Phys.* **2017**, *50*, 373002.

[27] L. K. Ono, Y. B. Qi, *J. Phys. Chem. Lett.* **2016**, *7*, 4764.

[28] S. Luo, W.A. Daoud, *J. Mater. Chem. A* **2015**, *3*, 8992.

[29] S. Shi, Y. Lic, X. Li, H. Wang, *Mater. Horiz.* **2015**, *2*, 378.

[30] K. Wang, C. Liu, C. Yi, L. Chen, J. Zhu, R. A. Weiss, X. Gong, *Adv. Funct. Mater.* **2015**, *25*, 6875.

[31] J. Xu, A. Buin, A. H. Ip, W. Li, O. Voznyy, R. Comin, M. Yuan, S. Jeon, Z. Ning, J. J. McDowell, P. Kanjanaboos, J.-P. Sun, X. Lan, L. N. Quan, D. H. Kim, I. G. Hill, P. Maksymovych, E. H. Sargent, *Nat. Commun.* **2015**, *6*, 7081.

[32] C.-H. Chiang, C.-G. Wu, *Nat. Photon.* **2016**, *10*, 196.

[33] G.-W. Kim, G. Kang, J. Kim, G.-Y. Lee, H. Il Kim, L. Pyeon, J. Lee, T. Park Lee, *Energy Environ. Sci.* **2016**, *9*, 2326.

[34] T. Kirchartz, K. Taretto, U. Rau, *J. Phys. Chem. C* **2009**, *113*, 17958.

[35] W. Chen, Y. Zhu, Y. Yu, L. Xu, G. Zhang, Z. He, *Chem. Mater.* **2016**, *120*, 4879.

[36] W. Yan, Y. Li, Y. Li, S. Ye, Z. Liu, S. Wang, Z. Bian, C. Huang, *Nano Res.* **2015**, *8*, 2474.

[37] L. S. Hung, C. W. Tang, M. G. Mason, *Appl. Phys. Lett.* **1997**, *70*, 152.

[38] H. Ding, Y. Geo, *Appl. Phys. Lett.* **2007**, *91*, 1.

[39] B. Hailegnaw, G. Adam, H. Heilbrunner, D. H. Apaydin, C. Ulbricht, N. S. Sariciftci, M. C. Scharber, *RSC Adv.* **2018**, *8*, 24836.

[40] P. Docampo, J. M. Ball, M. Darwich, G. E. Eperon, H. J. Snaith, *Nat. Commun.* **2013**, *4*, 1.

[41] S. Rothemund, I. Teasdale, *Chem. Soc. Rev.* **2016**, *45*, 5200.

[42] M. Deng, S. G. Kumbar, Y. Wan, U. S. Toti, H. R. Allcock, C. T. Laurencin, *Soft Matter* **2010**, *6*, 3119.

[43] A. Linhardt, M. König, W. Schöfberger, O. Brüggemann, A. K. Andrianov, I. Teasdale, *Polymers* **2016**, *8*, 161.

[44] J. Paulsdorf, N. Kaskhedikar, M. Burjanadze, S. Obeidi, N. A. Stolwijk, D. Wilmer, H.-D. Wiemhöfer, *Chem. Mater.* **2006**, *18*, 1281.

[45] I. Teasdale, *Eur. J. Inorg. Chem.* **2018**, *2019*, 1445.

[46] T. Mayer-Gall, D. Knittel, J. S. Gutmann, K. Opwis, *ACS Appl. Mater. Interfaces* **2015**, *7*, 9349.

[47] V. Poscher, I. Teasdale, Y. Salinas, *ACS Appl. Nano Mater.* **2019**, *2*, 655.

[48] C. G. Zoski, *Handbook of Electrochemistry*, Elsevier, Amsterdam, The Netherlands **2007**.

[49] C. M. Cardona, W. Li, A. E. Kaifer, D. Stockdale, G. C. Bazan, *Adv. Mater.* **2011**, *23*, 2367.

[50] D. Baran, A. Balan, S. Celebi, B. M. Esteban, H. Neugebauer, N. S. Sariciftci, L. Toppare, *Chem. Mater.* **2010**, *22*, 2978.

[51] L. Hu, K. Sun, M. Wang, W. Chen, B. Yang, J. Fu, Z. Xiong, X. Li, X. Tang, Z. Zang, S. Zhang, L. Sun, M. Li, *ACS Appl. Mater. Interfaces* **2017**, *9*, 43902.

[52] S. S. Mali, H. Kim, H. H. Kim, S. E. Shim, C. K. Hong, *Mater. Today* **2018**, *21*, 483.

[53] D. Prochowicz, M. M. Tavakoli, S.-H. Turren-Cruz, K. Pandey, M. Saliba, P. Yadav, *Sustainable Energy Fuels* **2018**, *2*, 2407.

[54] A. Pockett, G. E. Eperon, T. Peltola, H. J. Snaith, A. Walker, L. M. Peter, P. J. Cameron, *J. Phys. Chem. C* **2015**, *119*, 3456.

[55] A. Guerrero, G. Garcia-Belmonte, I. Mora-Sero, J. Bisquert, Y. S. Kang, T. J. Jacobsson, J. P. Correa-Baena, A. Hagfeldt, *J. Phys. Chem. C* **2016**, *120*, 8023.

[56] A. R. Pascoe, N. W. Du y, A. D. Scully, F. Huang, Y.-B. Cheng, *J. Phys. Chem. C* **2015**, *119*, 4444.

[57] A. Pockett, G. Eperon, N. Sakai, H. Snaith, L. M. Peter, P. J. Cameron, *Phys. Chem. Chem. Phys.* **2017**, *19*, 5959.

[58] X. Yin, P. Chen, M. Que, Y. Xing, W. Que, C. Niu, J. Shao, *ACS Nano* **2016**, *10*, 3630.